

High-resolution infrared imaging of the Red Rectangle nebula^{*}

D. Mékarnia¹, D. Rouan², E. Tessier³, C. Dougados³, and J. Lefèvre¹

¹ Observatoire de la Côte d'Azur, Département Fresnel, UMR CNRS 6528, B.P. 4229, F-06304 Nice Cedex 4, France

² Observatoire de Paris-Meudon, Département Spatial, URA CNRS 325, F-92195 Meudon Principal Cedex, France

³ Observatoire de Grenoble, Université Joseph Fourier, BP 53X, F-38041 Grenoble Cedex, France

Received 4 April 1997 / Accepted 27 May 1998

Abstract. We present the results of high angular resolution observations of the Red Rectangle nebula in the K(2.2 μm), L'(3.87 μm), M(4.75 μm) infrared bands and in the unidentified infrared (UIR) emission feature at 3.3 μm . The results confirm earlier near-infrared observations and show, with a better spatial resolution, that the bipolar structure of the object is still present very close to the core of the system at these wavelengths. The core of nebula is partially resolved in the K band and at 3.3 μm . We find that the UIR emission at 3.3 μm is enhanced along the cone walls. The images clearly show that the observed nebula is produced by a compact equatorial disk of dust slightly inclined with respect to the line of sight. Large particles are present in the circumstellar environment, probably both in the disk and in the lobes.

Key words: circumstellar matter – stars: evolution – stars: imaging – stars: individual: HD 44179 = Red Rectangle – stars: post-AGB – infrared: stars

1. Introduction

The Red Rectangle is a remarkable bipolar nebula associated with the 9th magnitude visible star HD 44179. The nebula has a rectangular aspect with a marked X-shaped morphology best seen in the red. It has attracted attention ever since it was first studied extensively by Cohen et al. (1975). HD 44179, the central star of the nebula, has been classified as a B9 to A0 III by Cohen et al. (1975), while Kelly & Latter (1995) identified its spectrum as that of an A1 III star.

The nature of the nebula and its central star HD 44179 are not well understood. Zuckerman et al. (1976) argue that the Red Rectangle is a proto-planetary nebula because of its unusual morphology, its carbon-rich nature, and the lack of interstellar material in the region. This interpretation is supported by polarization maps (Perkins et al. 1981) and by radiative transfer simulations (Yusef-Zadeh et al. 1984; Lopez et al. 1995,

1997). The possibility that HD 44179 is in a pre-main-sequence phase was first proposed by Cohen et al. (1975). This interpretation is consistent with the strong PAH emissions, also observed in pre-main-sequence stars (Brooke et al. 1993). On the other hand Waelkens et al. (1992) propose that the Red Rectangle is a post-main-sequence star because helium and/or carbon are over-abundant in HD 44179 relative to the solar values. However, the gas and dust in the circumstellar environment of the Red Rectangle are different from what they are around most carbon-rich red giants which are losing mass.

The Red Rectangle nebula is a powerful infrared source. Its infrared spectrum shows a smooth continuum much broader than that of a blackbody. It is featureless between 1.5 and 2.2 μm (Thronson 1982) and contains the entire family of the so-called unidentified infrared (UIR) emission features at 3.3, 6.2, 7.7, 8.6, and 11.3 μm (Russell et al. 1978). The width of the strong 3.3 μm feature is narrow near the central star (<2.7 arcsec) but then further away it becomes twice as wide (Geballe et al. 1989). A large variety of amorphous carbon and hydrocarbon solids have been proposed to explain the origin of UIR carriers but no identification definitely matches the observed spectra. This emission band is believed to be the result of absorption of ultraviolet photons followed by vibrational non-equilibrium excitation in the infrared.

High angular resolution speckle techniques have been many times applied to the Red Rectangle. These observations, performed in the infrared using either one-dimensional scans (Low 1979; Dyck et al. 1984; Dainty et al. 1985; Leinert & Haas 1989) or two-dimensional data (Christou et al. 1990; Tessier et al. 1990; Cruzalèbes et al. 1996), show the Red Rectangle to be a clearly extended source in the north-south direction. Dyck et al. (1984) observed in the near-infrared (1.65–4.8 μm) and resolved the central source into two components: an extended (0.9 arcsec) component and a compact one. Dainty et al. (1985) found that the extended emission is elongated (1.05 arcsec) in the north-south direction (vs 0.4 arcsec in the east-west direction) in K, L and M bands. Leinert and Haas (1989) performed a tomographic image reconstruction at K. They resolved the central compact source into two components: a 0.2 arcsec source and an unresolved component offset by 0.15 arcsec to the south, which they identified with the star HD 44179. The K image obtained by Christou et al. (1990) clearly shows two sources with

Send offprint requests to: D. Mékarnia, (mekarnia@obs-nice.fr)

^{*} Based on observations collected at the Canada-France-Hawaii Telescope, operated by the National Research Council of Canada, the Centre National de la Recherche Scientifique of France, and the University of Hawaii.

a 0.15 arcsec separation at a position angle of 13° . Using an adaptive optics technique Roddier et al. (1995) show that the Red Rectangle has an X-shaped morphology within 0.1 arcsec of the central region of the system at $1.65 \mu\text{m}$. Recently Osterbart et al. (1997) performed high resolution images at $0.656 \mu\text{m}$ and at $0.80 \mu\text{m}$ of the nebula. They have resolved the central part of the nebula into two main lobes, which appear separated by about 0.15 arcsec. Cruzalèbes et al. (1996) found some east-west components in K and M. In addition, Bregman et al. (1993) obtained images of the Red Rectangle in the 3.3 and $11.3 \mu\text{m}$ UIR emission bands. These images show two different spatial distributions: the $3.3 \mu\text{m}$ image is slightly extended in the north-south direction and centrally peaked, while the $11.3 \mu\text{m}$ image shows a north-south bipolar shape with no central peak. Geballe et al. (1989) detected $3.3 \mu\text{m}$ UIR emission in a 5 arcsec beam centered north of HD 44179. Sloan et al. (1993) showed that the object is spatially extended at the wavelengths of all four UIR features detected between 7 and $14 \mu\text{m}$ and found that no UIR emission arises in the innermost regions of the source. Images of the Red Rectangle were obtained at UIR emission features and at several continuum wavelengths in the $10 \mu\text{m}$ and $20 \mu\text{m}$ atmospheric windows by Hora et al. (1996). The nebula was seen to follow the optical morphology. The “spikes”, or brightness enhancements, that give the nebula its rectangular appearance have also been observed at $10 \mu\text{m}$. The mid infrared emission appears to be trace material in the bipolar outflow regions of the nebula. Knapp et al. (1995) found an unresolved (<3 arcsec) CO emission associated with the central star which they attribute to ionized gas corresponding to a star earlier than B3. Recently Jura et al. (1997) performed radio VLA observations at 3.6 cm, 2 cm and 1.3 cm of the Red Rectangle. Emission was detected in all three radio wavelengths, and the source was resolved at 2 cm and 1.3 cm. They suggest that the radio emission is produced by large particles confined to a long-lived gravitationally bound disk.

There have been many discussions about the nature of the binarity of the central star of the nebula which has long been considered as a visual binary. Meaburn et al. (1983) estimated the separation to be 0.29 arcsec while Heintz (1990) measured a separation of only 0.14 arcsec. Radial velocity (Van Winckel et al. 1995) and photometric measurements (Waelkens et al. 1996) show that HD 44179 is a spectroscopic binary while adaptive optics measurements (Roddier et al. 1995) provide indirect evidence that the source is a binary star. It seems more probable that the claimed companion seen in visual observations is reflected light of the nebula, as already proposed by Cohen et al. (1975) and by Roddier et al. (1995).

In order to probe the geometry of the circumstellar material in the close environment of the Red Rectangle we have obtained high resolution infrared images at K ($2.22 \mu\text{m}$), L' ($3.87 \mu\text{m}$), M ($4.75 \mu\text{m}$) bands and in the $3.3 \mu\text{m}$ UIR emission band. The primary goals of this study are to investigate the nature of the circumstellar dust grains and to develop a better understanding of the formation and structure of this source. In Sect. 2, we describe the observations and the data processing. In Sect. 3, we present the results. In Sect. 4 we discuss the intensity and

the morphology we have derived from observations and finally, we summarize our conclusions in Sect. 5.

2. Observations and data reduction

The observations presented here were carried out at the 3.6m CFHT (Canada-France-Hawaii Telescope) on 19 and 20 April 1995 in good seeing conditions (between 0.3 and 0.6 arcsec FWHM in the visible) with the INSU-OPM (Institut National des Sciences de l'Univers, Observatoire de Paris-Meudon) infrared camera CIRCUS. The CIRCUS camera included a 128×128 InSb array detector which was optimized for the thermal infrared bands ($\lambda \geq 3 \mu\text{m}$). The camera was used in speckle mode data acquisition i.e. single exposures were kept relatively short. Measurements were made in the K ($\lambda_o=2.22 \mu\text{m}$, $\Delta\lambda=0.36 \mu\text{m}$), L' ($\lambda_o=3.87 \mu\text{m}$, $\Delta\lambda=0.61 \mu\text{m}$), M ($\lambda_o=4.75 \mu\text{m}$, $\Delta\lambda=0.43 \mu\text{m}$) bands and in the UIR emission band ($\lambda_o=3.3 \mu\text{m}$, $\Delta\lambda=0.16 \mu\text{m}$).

The speckle data include a set of short exposure images of the source, an unresolved reference star and their adjoining sky backgrounds. The nearby star SAO 133091 was used as a point source to determine the point spread function (PSF). We switched every few minutes between the object and the reference star in order to sample the temporal seeing variations so as to minimize seeing effects during the reduction process. The reference star was chosen to have brightness similar to that of the source. Proximity in the sky and similarity in brightness of the reference was chosen in order to prevent non-linear effects due to the detector defects or to the variation of the optical transfer function.

During the observations, we used a 64×64 sub-array of the detector selected for its best performances. The magnification was 0.109 arcsec per pixel which gave a field of view of $6.4 \times 6.4 \text{ arcsec}^2$. The integration time was selected to achieve the best resolution with a sufficiently large signal-to-noise ratio. We made images with exposure time of 147 ms in K and L', 183.9 ms in the M band and 294.6 ms at $3.28 \mu\text{m}$. In order to estimate the contribution of the detector and of the sky we used the same integration time for the sky close to the source (typically 40 arcsec away) and reference frames for each bandwidth. The journal of observations is given in Table 1.

Data were analyzed using the package developed by Tessier (1993) within IRAF by the following procedure. Each image first had the background subtracted and was interpolated over bad pixels. The best images of the source were then co-added using the shift-and-add (SAA) technique. The SAA images were therefore deconvolved using PSF's derived from similar data for the reference star. We used the IRAF Lucy algorithm to deconvolve images. The angular resolution after image reconstruction is of ~ 0.2 arcsec at K, L' and $3.3 \mu\text{m}$, and ~ 0.3 arcsec at M.

The spatial calibration was determined from the binary star δ Ser giving an absolute spatial scale better than 1% and a position angle (PA) less than 1 degree. No photometric calibrations have been done.

Our $3.3 \mu\text{m}$ UIR image is obtained through a so-called PAH filter centered at $3.28 \mu\text{m}$ with a spectral width of $0.16 \mu\text{m}$.

Table 1. Journal of observations

Date	$\lambda(\mu\text{m})$	$\Delta\lambda(\mu\text{m})$	Number of frames	Total exposure time (s)
1995 April 19	2.22	0.36	640	94
1995 April 19	3.28	0.16	384	113
1995 April 20	3.87	0.61	640	94
1995 April 20	4.75	0.43	384	70

The filter contains not only the UIR feature but also a continuum which was not subtracted. From Geballe et al. (1989), we estimate the contribution from the continuum in this filter at approximately 60 % of the PAH emission.

3. Results

Fig. 1 shows contour plots for the resulting images of the Red Rectangle. The plots appear to be similar at a first look but provide several detailed features that we describe briefly:

1. The central region (0.5 arcsec) of the nebula is elongated along a nearly north-south direction. L' and M images are similar while the one at 3.3 μm is more elongated and the K image is more symmetric.
2. In K band and at 3.3 μm the core of the nebula is partially resolved into two sources with an angular separation less than 0.2 arcsec. In Fig. 2, we display the east-west photometric profiles through the maximum along the north-south direction of each image (the maxima have been normalized to the same value). The L' and 3.3 μm images have relatively brighter cores (with respect to the extended component) than the K and M images.
3. The X shape of the nebula already seen at small scales (0.1 arcsec) at 0.85 μm and 1.65 μm (Roddier et al. 1995) is clearly visible in our images. The axis of the cone is oriented with a P.A. of 13°. The opening angle of the cone increases with wavelength. The cone is less open ($\sim 60^\circ$) in the K image than in the M image ($\sim 80^\circ$). This is shown in detail in Fig. 3 where low values of the intensities close to the core are plotted. The image at 3.3 μm shows that the UIR emission is more prominent along the walls of the bicone than the continuum. This confirms the mid-infrared UIR observations of Hora et al. (1996) and is the first observation of this structure at a wavelength of 3.3 μm .
4. The nebula is not axisymmetric. All images present an asymmetry of the inner lobes, with the southern lobe being about 50% brighter than the northern one. These images favour a geometry where the system is tilted a few degrees out of the plane of the sky causing the northern lobe to be obscured by dust in the equatorial disk. Table 2 gives estimates of the relative contribution of the total flux at each wavelength in the core and the north and south lobes. Fig. 4 shows the geometry used to calculate these flux contributions.
5. No stellar binarity appears in any image.

Table 2. Relative flux contributions in the Core, the South and the North lobe of the total flux in K, L', M and at 3.3 μm . See Fig. 2 for the geometry description of the extension of the core and the two lobes.

	K	L'	M	3.3 μm
Core	24%	30%	28%	26%
North lobe	22%	21%	24%	21%
South lobe	54%	49%	48%	53%

6. A structure extending to about 0.5 arcsec from the core of the nebula is present in the eastern direction of the K image. This structure is also present in the K image of Cruzalèbes et al. (1996) and in the H image of Roddier et al. (1995). On the other hand there are no significant east-west features in our L' & M images.

4. Discussion

The bipolar structure of the Red Rectangle is located very close to the core of the system. This structure suggests the existence of an equatorial disk and is consistent with the current model of a carbon-rich post-AGB star evolving into the planetary nebula phase (Van Winckel et al. 1995; Roddier et al. 1995; Lopez et al. 1995, 1997). Our results reveal clear similarities between images taken at 2.2 μm and at 3.3 μm UIR on the one hand, and between L' and M images on the other hand. In addition, our K image is similar to the H image of Roddier et al. (1995). There is also good correlation between our 3.3 μm UIR image and UIR mid-infrared images of Hora et al. (1996). The north-south extension of the nebula is largest at shorter wavelengths (H, K) and smallest at longer wavelengths (L', M & N). The “spikes” which are so striking at H become progressively less apparent as the wavelength is increased. However, all infrared images of the nebula are north-south elongated. This could be an indication that scattering is more efficient in the polar direction. We assume that at shorter wavelengths the overall feature is dominated by scattering whereas long wavelength images display both scattering and dust emission. The scattering begins to be quite efficient in the near infrared when the grain size distribution function contains particles greater than 1 μm while larger particles are needed to explain the scattering efficiency

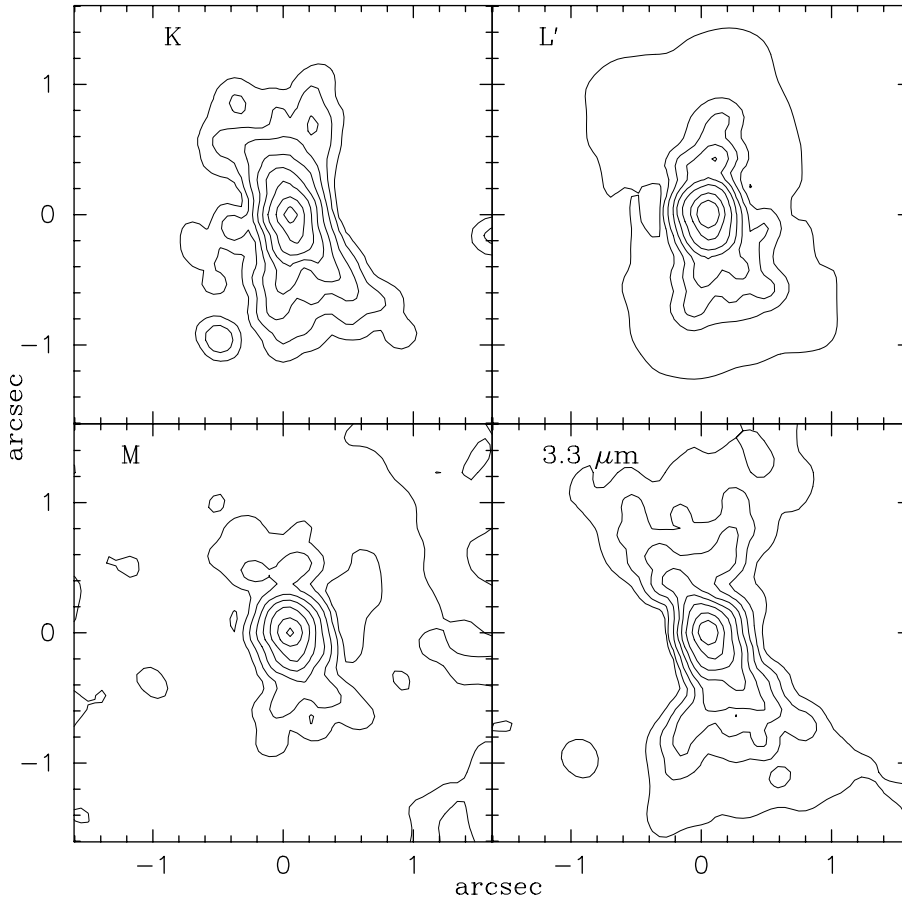


Fig. 1. Contour plots of the intensity of the K ($2.22 \mu\text{m}$), L' ($3.87 \mu\text{m}$), M ($4.75 \mu\text{m}$) and $3.3 \mu\text{m}$ UIR feature deconvolved images of the Red Rectangle. North is at the top and East is on the left. Contour levels are 2, 1, 0.4, 0.2, 0.1, 0.04 and 0.012% of the total power for each image. Lowest contours are five times the standard deviation of the noise, measured in regions external to the nebula.

observed at longer wavelengths. The main issue of the physical interpretation of these results is what causes the apparent X-shaped morphology or at least the rectangular shape present in infrared images of the nebula. Is it due to the spatial distribution of the dust density and/or of the size distribution of the grains or is it due to other physical conditions? We suggest that the observed X-shaped morphology is produced by the scattering of dust grains in a compact equatorial thick disk with evacuated polar regions. Large grains are present not only in the equatorial plane (as proposed by Cohen et al. 1975; Jura et al. 1995, 1997 and by Lopez et al. 1995, 1997) but also in the lobes. The increase of the opening angle with wavelength seen in our images could indicate that large grains are mostly located at the outer edges of the cavity walls and supports the scenario proposed by Jura et al. (1997). In fact, according to Jura et al. (1997) large carbon particles up to 0.02 cm in diameter are confined in a long-lived disk around the star. In such an orbiting disk, grain-grain collisions create and eject a whole range of possible species including small and large particles. The X-shaped structure, observed close to the core of the system, could be produced by the dust that is pushed outwards by expanding gas. Material ejected in the outflow or formed by interaction of the outflow with the dust may condense along the cone walls giving the observed lobes (Roddier et al. 1995).

Our $3.3 \mu\text{m}$ UIR image is elongated along the cone walls of the nebula while Bregman et al. (1993), who performed imag-

ing at $3.3 \mu\text{m}$ and at $11.2 \mu\text{m}$, found the $3.3 \mu\text{m}$ image to be centrally peaked. However, the lower resolution of their $3.3 \mu\text{m}$ image did not allow them to detect the morphological features present in our image. UIR images obtained by Hora et al. (1996) at $8.0 \mu\text{m}$, $8.6 \mu\text{m}$ and $11.2 \mu\text{m}$ display a shape similar to our $3.3 \mu\text{m}$ image and are more elongated than the mid-infrared continuum emission. According to Hora et al. (1996), the mid-infrared emission appears to be trace material in the bipolar outflow regions, rather than in an equatorial density enhancement.

The hypothesis of a compact equatorial disk with a polar free cavity which collimates a mass outflow driven by radiation is consistent with our $3.3 \mu\text{m}$ image. Hence, if the dust grains causing the scattering are different from the UIR particles, then UIR images may will be the result of the excitation of these particles by the ultraviolet radiation of the central star.

No binarity in the system is seen in our data. It is more likely that the inner structure of the bipolar lobes of the nebula has been misinterpreted by visual observers as a double star (see Roddier et al. 1995). The hypothesis that the bipolar nebula was created from a binary system by tidal interaction between the secondary and the expanding red giant primary was proposed by Morris (1981) and Roddier et al. (1995) while Yusef-Zadeh et al. (1984) and Lopez et al. (1995, 1997) proposed a model where a single star is surrounded by an axisymmetric dust shell. Models of the Red Rectangle obtained by Lopez et al. (1997) which use radiative transfer simulations, reproduce the spectral

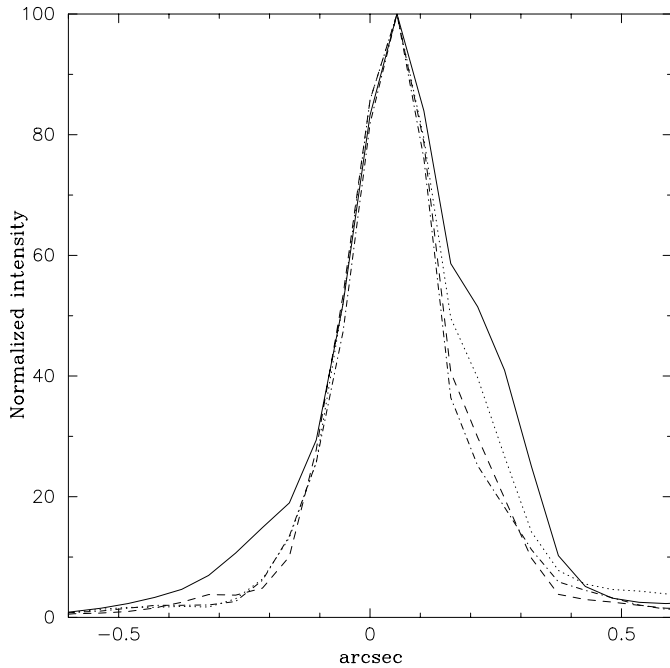


Fig. 2. Photometric profiles of the deconvolved images of the core of the Red Rectangle nebula in the direction of the side lobes ($PA = 13^\circ$). The vertical intensity scale is arbitrary. Profiles have been normalized to the same maximum intensity. North is on the right hand side. Full line: K image; dash: L' image; dash-dot: M image; dot: $3.3 \mu\text{m}$ image. Both lobes are partially resolved in K and at $3.3 \mu\text{m}$.

energy distribution and both visible (on scales of some arcsec) and $2.2 \mu\text{m}$ images of the nebula quite well. However Lopez et al. (1997) have difficulty in fitting both the visible and infrared shapes with the same set of model parameters. The main result of their study is the presence of large particles in the circumstellar environment of the nebula, with sizes greater than or equal to $1.2 \mu\text{m}$.

5. Conclusion

High angular resolution images of the Red Rectangle nebula have been obtained in the near infrared K, L', M bands and in the unidentified infrared (UIR) emission feature at $3.3 \mu\text{m}$. These images show, for the first time at these wavelengths, that the spikes or brightness enhancements are present very close to the core of the system. All images are slightly elongated along a nearly north-south direction and generally have a similar aspect. The K image presents a symmetrical aspect while the L' and M images are less north-south extended. The $3.3 \mu\text{m}$ UIR image is more elongated than the K, L' and M images. The core of the nebula is partially resolved in K and at $3.3 \mu\text{m}$. No binary structure is present in our data.

Our results confirm earlier near-infrared observations and are consistent with a model of the nebula in which a central star is surrounded by a compact and thick equatorial disk of dust with evacuated polar regions. The disk is probably a long-lived disk, slightly tilted away from the line of sight, with large grains as proposed by Jura et al. (1995, 1997). We suggest that large

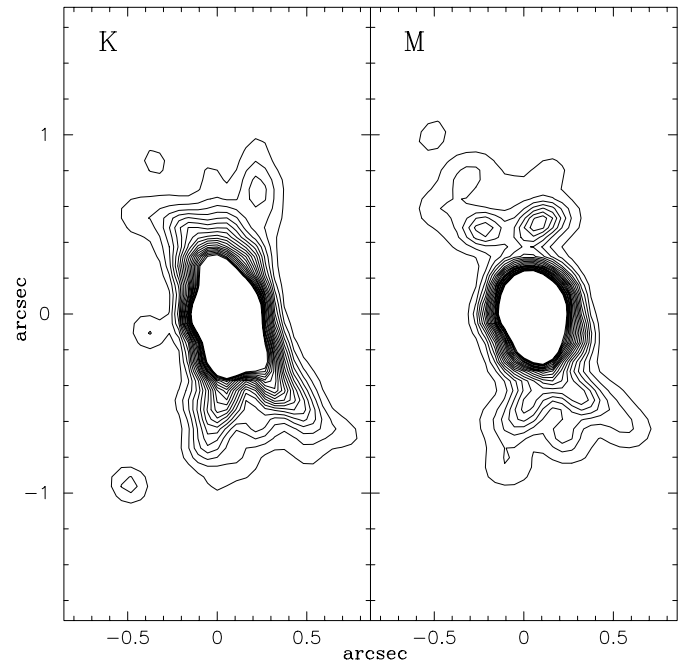


Fig. 3. Contour plot of the intensity in the core of the K and M images of the Red Rectangle. North is at the top, east is on the left. In K, the cone seems less open (with a total angle of $\sim 60^\circ$) than in M ($\sim 80^\circ$).

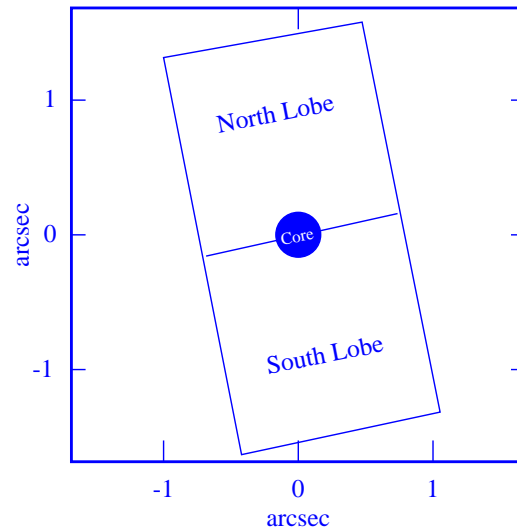


Fig. 4. Geometry used to calculate the relative flux contributions of the core and of the South and North lobes to the total flux. The central core is 0.21 arcsec in diameter while the two lobes cover an area of approximately $1.5 \times 1.5 \text{ arcsec}^2$.

grains are also present in bipolar outflow regions. However, it is clear that a detailed interpretation requires high angular resolution observations as well as a consistent treatment of radiative transfer.

Acknowledgements. We would like to thank the CIRCUS team of the Observatoire de Paris, and especially F. Lacombe and S. Pau for their assistance during the observations. We are grateful to our referee Massimo Robberto for his helpful comments. We also thank Bruno Lopez and John Tully for their reading of the manuscript. This research

has made use of the Simbad database, operated at CDS, Strasbourg, France.

References

- Bregman, J.D., Rank, D., Temi, P., Hudgins, D., & Kay, L. 1993, *ApJ*, 411, 794
- Brooke, T.Y., Tokunaga, A.T., & Strom, S.E. 1993, *AJ*, 106, 656
- Christou, J.C., Ridgway, S.T., Busher, D.F., Haniff, C.A., Mc Carthy Jr. D.W., 1990, *Astrophysics with Infrared Arrays*, Ed. Elston (ASP Conf. Series 14), 133
- Cohen, M., Anderson, C.M., Cowley, A., Coyne, G.V., Fawley, W.M., Gull, T.R., Harlan, E.A., Herbig, G.H., Holden, F., Hudson, H.S., Jakoubek, R.O., Johnson, H.M., Merrill, K.M., Schiffer F.H., Soifer, B.T., Zuckerman, B. 1975, *ApJ*, 196, 179
- Cruzalèbes, P., Tessier, E., Lopez, B., Eckart, A. & Tiphène D. 1996, *A&AS*, 116, 597
- Dainty, J.C., Piher, J.L., Lacasse, M.G., Ridgway, S.T. 1985, *ApJ*, 293, 530
- Dyck, H.M., Zuckerman, B., Leinert, C., Beckwith, S. 1984, *ApJ*, 287, 801
- Geballe, T.R., Tielens, A.G.G.M., Allamandola, L.J., Moorhouse, A., Brand, P.W.J.L. 1989, *ApJ*, 341, 278
- Heintz, W.D. 1990, *MNRAS*, 245, 759
- Hora, J.L., Deutsch, L.K., Hoffmann, W.F, Fazio, G.G. 1996, *AJ*, 112, 2064
- Jura, M., Balm, S.P., Kahane, C. 1995, *ApJ*, 453, 721
- Jura, M., Turner, J. & Balm, S.P. 1997, *ApJ*, 474, 741
- Kelly, D.M., Latter, W.B. 1995, *AJ*, 109, 1320
- Knapp, G.R., Bowers, P.F., Young, K. & Phillips, T.G. 1995, *ApJ*, 455, 293
- Leinert, C. & Haas, M. 1989, *A&A*, 221, 110
- Lopez, B., Mékarnia, D., Lefèvre, J. 1995, *A&A*, 296, 752
- Lopez, B., Tessier, E., Cruzalèbes, P., & Lefèvre, J. & T. Le Bertre 1997, *A&A*, 322, 868
- Low, F.J. 1979, in *IAU Colloquium 50, High Angular Resolution Stellar Interferometry* Eds. J. Davis & W.J. Tango, Sidney, p.15-1
- Meaburn, J., Walsh, J.R., Hebden, J.C., Morgan, B.L., Vine, H., 1983, *MNRAS*, 205, 53
- Morris, M., 1981, *ApJ*, 249, 572
- Osterbart, R., Langet, N. & Weigelt, G. 1997, *A&A*, 325, 609
- Perkins, H.G., Scarrott, S.M., Murdin, P. & Bingham, R.G. 1981, *MNRAS*, 196, 635
- Roddier, F., Roddier, C., Graves, J.E., & Northcott, M.J. 1995, *ApJ*, 443, 249
- Russell, R.W.; Soifer, B.T.; & Willner, S.P. 1978, *ApJ*, 220, 568
- Sloan, G.C., Grasdalen, G.L., & LeVan P.D. 1993, *ApJ*, 409, 412
- Tessier E., Perrier, C., Léna, P., Michel, C., Langlet, A. 1990, in *ASP Conference Series, Astrophysics with Infrared Arrays*, Vol.14, Ed. R. Elston, 145
- Tessier E. 1993, *PHD Thesis*, Université de Paris 6
- Thronson, H.A., JR. 1982, *AJ*, 87, 1207
- Van Winckel, H., Mathis, J.S., & Waelkens, C. 1992, *Nature*, 356, 500
- Van Winckel, H., Waelkens, C. & Waters, L.B.F.M. 1995, *A&A*, 293, L25
- Waelkens, C.; Van Winckel, H.; Trams, N.R. & Waters, L.B.F.M. 1992, *A&A*, 256, L15
- Waelkens, C.; Van Winckel, H.; Waters, L.B.F.M. & Bakker E.J., 1996, *A&A*, 314, L17
- Yusef-Zadeh F., Morris, M. & White, R.L. 1984, *ApJ*, 278, 186
- Zuckerman, B., Gilra, D.P., Turner, B.E., Morris, M., & Palmer, P. 1976, *ApJ*, 205, L15